Operating temperatures of oil-lubricated medium-speed gears: numerical models and experimental results

H Long, A A Lord, D T Gethin* and **B J Roylance**
Department of Mechanical Engineering, University of Wales Swansea, Wales, UK

Abstract: This paper investigates the effects of gear geometry, rotational speed and applied load, as well as lubrication conditions on surface temperature of high-speed gear teeth. The analytical approach and procedure for estimating frictional heat flux and heat transfer coefficients of gear teeth in high-speed operational conditions was developed and accounts for the effect of oil mist as a cooling medium. Numerical simulations of tooth temperature based on finite element analysis were established to investigate temperature distributions and variations over a range of applied load and rotational speed, which compared well with experimental measurements. A sensitivity analysis of surface temperature to gear configuration, frictional heat flux, heat transfer coefficients, and oil and ambient temperatures was conducted and the major parameters influencing surface temperature were evaluated.

Keywords: tooth temperature, frictional heating, convection heat transfer, finite element temperature analysis, spur gear transmission

NOTATION

$2a$	contact width (mm)
b	tooth width (mm)
c	specific heat (J/kg K)
C_S, C_L	constants in temperature exponential equations
d	weighting factor of the heat transfer coefficient
d_a, d_{a1}, d_{a2}	tip diameters (mm)
d_{b1}, d_{b2}	base diameters (mm)
d_1, d_2	pitch diameters (mm)
E	equivalent Young's modulus (N/mm^2)
F_{Nc}, F_{tc}	normal and tangential forces at contact point C (N)
g_{yc}	distance of meshing point C from the pitch point (mm)
h_s, h_{tc}	heat transfer coefficients of the gear surface and tooth flank (W/m^2 K)
H_c	height of point C on the tooth (mm)
k	conductivity
m	exponent constant in a wall temperature distribution
m, n	exponential constants in temperature equations
n_1, n_2	rotational speeds of the pinion and gear shafts (r/min)
Nu, Pr, Re	Nusselt, Prandtl and Reynolds numbers
p_{Nc}	average normal contact pressure at point C (N/mm^2)
q_c, q_{1c}, q_{2c}	frictional heat flux (W/m^2)
q_F	frictional heat flux on the meshing flank (W/m^2)
q_{1ave}, q_{2ave}	average frictional heat flux of the pinion and gear (W/m^2)
r_c	radius of contact point C on the pinion (mm)
R_{a1}, R_{a2}	tip radii of the pinion and gear (mm)
R_{E1}, R_{E2}	radii of contact point curvature in the pinion and gear (mm)
R_{Ec}	equivalent curvature radius of meshing points (mm)
$T(x, y, z)$	tooth temperature (°C)
T_a, T_{oil}	ambient and oil inlet temperatures (°C)
$T_{s,max}$	maximum surface temperature of the tooth (°C)
V_{gc}	sliding velocity of the meshing points (m/s)
V_{1C}, V_{2C}	velocities of point C in the contact tangent direction (m/s)
X_R	roughness factor
α	pressure angle
	thermal diffusivity $= \kappa/(\rho c)$

The MS was received on 12 March 2001 and was accepted after revision for publication on 12 February 2003.
* *Corresponding author: Department of Mechanical Engineering, University of Wales Swansea, Singleton Park, Swansea SA2 8PP, Wales, UK.*

α_a, α_o	average volume fractions occupied by air and oil on the gear surfaces
γ	heat conversion factor
$\partial T/\partial n$	temperature gradient
ζ	properties of the synthesized fluid of air and oil
η	dynamic viscosity (N s/m)
θ_B	estimated bulk temperature (°C)
κ	thermal conductivity (W/m K)
μ_c	coefficient of friction
ν	Poisson's ratio
	kinematic viscosity (m^2/s)
ρ	density (kg/m^3)
ω	rotational speed $= 2\pi n$

Subscripts

b_1, b_2	insulated surfaces of the gear model
f, a, o	synthesized fluid, air and oil
m, t, s	meshing flank, non-working flank and surface of gear
B, T	bulk and flash temperatures of the gear tooth
1, 2	pinion and gear

1 INTRODUCTION

Tooth surface temperature has a significant effect on gear performance and failure in high-speed gear transmissions for aerospace applications. Tooth temperature and thermal behaviour of gears are affected by gear geometry, rotational speed, applied load, lubrication and operational conditions. Gear parameters and tooth profile have direct influences on load sharing and pressure distribution, and tooth sliding along the contact path of the meshing teeth. Relative sliding of the meshing teeth under high-speed conditions results in significant frictional heat generation, which is determined by the load sustained, rotational speed and coefficient of friction. Heat generated is conducted into the gear teeth and is also taken away by the cooling lubricant applied on the gear wheel and tooth flank. Heat transfer coefficients change with the rotational speed, surface location and operational conditions such as the flowrate of the lubrication oil, the temperature of the oil inlet and the position of the oil jet. The frictional heat flux generated on the tooth flank and heat transfer on the gear surfaces and tooth flanks have a significant influence on the temperature variation and distributions. Consequently they affect gear lubrication, performance and service life.

Experimental techniques, theoretical approaches and numerical modelling methods have been used to investigate interactions in relation to heat generation, heat transfer and lubrication effects under combined conditions of rotational speed and load. However, it has been difficult to predict tooth temperature and evaluate thermal behaviour of gear transmission systems, since thermal balance and gear temperature are determined by a number of factors including gear parameters and configuration, applied loads and rotational speeds, as well as lubricant properties and operating conditions.

Townsend and Akin [**1**] have conducted tooth temperature analysis of a spur gear using the finite element method with calculation of heat input and estimation of heat transfer coefficients as well as experimental measurements using the infrared radiometric microscope. The effects of oil pressure on jet cooling, oil inlet temperature and oil jet impingement depth with consideration of load applied and operating speed on average and surface temperatures have been investigated in their research. A numerical and analytical approach to gear dynamic load, lubricant film thickness, bulk equilibrium and total flash temperatures in spur gear contacts has been developed by Wang and Cheng [**2**]. The distribution of bulk equilibrium temperature and flash temperature along the contact path for pinion and gear teeth were derived and the influences of face width, outside radius and pitch diameter were evaluated [**3**]. This approach has been extended to include the effects of non-uniform convective heat transfer coefficients over the surfaces of gear teeth with heat transfer analysis by Patir and Cheng [**4**]. The theoretical calculation of surface temperature of spur gear teeth was compared with experimentally measured values with consideration of affected factors, such as transmission errors of test gears and total stiffness of gear teeth, on the dynamic loads by Terauchi and Mori [**5**]. However, a general approach to temperature analysis for engineering applications and an investigation of the impacts of operational conditions on surface temperature are currently limited.

The development of an analysis approach and modelling procedure to evaluate thermal behaviour and tooth temperature under high-speed operation conditions is described in this paper. Frictional heat generation at the meshing teeth along the contact path and convective heat transfer coefficients of gear surfaces and tooth flanks were estimated and analysed. Three-dimensional finite element (FE) models of the gear tooth were established to investigate temperature distributions and variations along the contact path over a range of applied loads and operating speeds with consideration of lubrication conditions.

In this paper it will be shown that surface and tooth temperatures under steady state predicted by finite element analysis are in good agreement with experimental measurements obtained using an infrared camera and thermocouples. FE analysis results suggested that the maximum surface temperature and temperature distributions on the tooth flank are mainly determined

by load and speed as well as gear geometrical configuration. However, load has a more significant effect on the surface temperature in comparison with the rotational speed. Sensitivity analysis of the surface temperature to relevant variables revealed that tooth width has an important impact on tooth temperature variations and distributions. Ambient temperature under operational conditions is an essential parameter to define boundary conditions in FE models and it has a proportional effect on the temperature prediction under steady state conditions. A precise calculation of the local frictional heat flux is required to predict tooth temperature accurately.

2 ANALYSIS APPROACH AND MODELLING PROCEDURE

Within the gear contact, at steady state, the frictional heat generated is balanced by the heat removal processes. These key mechanisms will be discussed in the follow sections.

2.1 Frictional heat generation

Frictional heat generation during gear meshing is determined by the applied load, rotational speed and lubrication on the tooth flank. The frictional heat flux varies over the tooth flank due to changes of sliding velocity, normal contact pressure and the coefficient of friction along the contact path. These issues will be discussed fully in the following subsections.

2.1.1 Gear meshing and contact pressure

The use of involute teeth in gears provides uniform transmission of motion and a constant direction of the tooth normal force during meshing. The contact of a spur gear pair commences as the root of the driving gear engages with the tip of the driven gear (B_2), while the leading pair of teeth is engaged at the exit point of single tooth contact (E_1), as shown in Fig. 1.

As the leading pair of teeth is approaching the exit point of contact (B_1), the current pair of teeth is at the entry point of single tooth contact (E_2). The applied load on the gears is shared between pairs of teeth engaged simultaneously in the zone of double-tooth contact along the contact path and by one pair of teeth within the single-contact zone. Therefore, the normal force applied on the tooth changes with the meshing process and produces a non-uniform contact pressure distribution on the tooth flank. Gear teeth with properly modified profiles can eliminate the sudden variation in load and reduce tooth meshing impact and gear vibration.

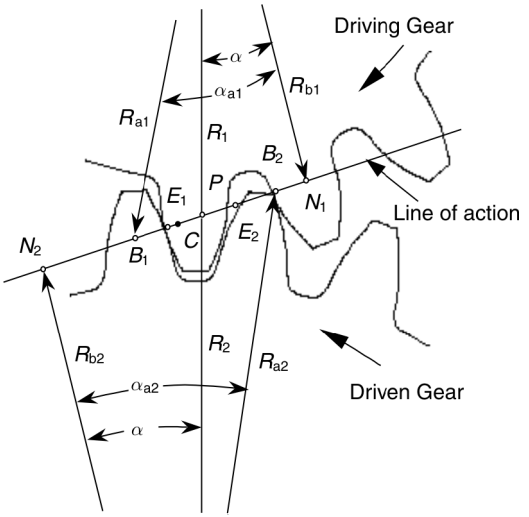

Fig. 1 Meshing process and contact analysis

In order to evaluate variations of the normal force on the tooth along the contact path and analyse its effect on frictional heat flux, the distance between the instant meshing point with the pitch point (defined as P in Fig. 1) on the line of action has to be calculated. The positions of the start and the end of the meshing points on the contact path defined utilizing part of the line of action, PB_1 and PB_2, can be written as

$$PB_1 = \sqrt{\tfrac{1}{4}\left(d_{a1}^2 - d_{b1}^2\right)} - \tfrac{1}{2}d_1 \sin\alpha \tag{1}$$

$$PB_2 = \sqrt{\tfrac{1}{4}\left(d_{a2}^2 - d_{b2}^2\right)} - \tfrac{1}{2}d_2 \sin\alpha \tag{2}$$

The distance between an arbitrary meshing point, C, on the pinion with radius of r_c with the pitch point along the contact path, g_{yc}, can be expressed as

$$g_{yc} = \mp\tfrac{1}{2}d_1 \sin\alpha \pm \sqrt{\left(\tfrac{1}{2}d_1 \sin\alpha\right)^2 - \left(\tfrac{1}{2}d_1\right)^2 + r_c^2} \tag{3}$$

The upper sign is for a contact point on the addendum flank of the pinion or the dedendum flank of the gear. The lower sign is for a contact point on the dedendum flank of the pinion or the addendum flank of the gear.

The normal contact pressure on the tooth flank was determined by the normal force applied on the tooth, gear material properties and the tooth profile. Based on the Hertzian contact theory, the average compressive pressure for an arbitrary meshing pair of teeth, p_{Nc}, as shown in Fig. 2, which is typical for a gear pair without tip relief, can be expressed as

$$p_{Nc} = \frac{\pi}{4}\sqrt{\frac{F_{Nc}E}{2\pi R_{Ec} b(1-\nu^2)}} \tag{4}$$

The equivalent radius of curvature for the meshing pair of teeth, R_{Ec}, represents the effect of contact position change on the contact pressure due to the variation of

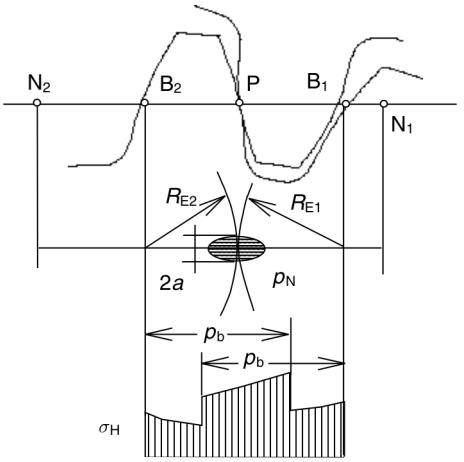

Fig. 2 Contact pressure of meshing teeth

the equivalent radius of curvature of the mating teeth profiles. It can be expressed as

$$R_{\mathrm{Ec}} = \frac{R_{\mathrm{E1}} R_{\mathrm{E2}}}{R_{\mathrm{E1}} + R_{\mathrm{E2}}}$$
$$R_{\mathrm{E1}} = \tfrac{1}{2} d_1 \sin\alpha \pm g_{\mathrm{yc}}$$
$$R_{\mathrm{E2}} = \tfrac{1}{2} d_2 \sin\alpha \mp g_{\mathrm{yc}} \tag{5}$$

The meaning of the upper/lower sign used in equations (5) is the same as the sign used in equation (3).

2.1.2 *Sliding velocity and coefficient of friction*

The differences in rotational speed and sizes of the pinion and gear result in unequal velocities of the pinion and gear in the direction of motion. Therefore, absolute velocities of the meshing teeth on the pinion and gear in the direction of contact tangents are different and consequently relative sliding between the tooth flanks of the pinion and gear occurs. However, the absolute velocities of the pinion and gear in the direction of the contact normal are identical, which provides a constant transmission of motion during engagement. Tooth sliding is important for frictional heating and tooth wear. The absolute velocities of the meshing points on the pinion and gear in the direction of contact tangents, $V_{1\mathrm{c}}$ and $V_{2\mathrm{c}}$, and the sliding velocity of the meshing points, V_{gc}, can be expressed as

$$V_{1\mathrm{c}} = \frac{2\pi n_1 \left(\frac{1}{2} d_1 \sin\alpha \pm g_{\mathrm{yc}}\right)}{60 \times 1000}$$
$$V_{2\mathrm{c}} = \frac{2\pi n_2 \left(\frac{1}{2} d_2 \sin\alpha \mp g_{\mathrm{yc}}\right)}{60 \times 1000}$$
$$V_{\mathrm{gc}} = V_{1\mathrm{c}} - V_{2\mathrm{c}} = \frac{\pm 2\pi n_1 g_{\mathrm{yc}} (1 + d_1/d_2)}{60 \times 1000} \tag{6}$$

The meaning of the upper/lower sign used here is the same as that explained for equation (3).

Power loss in the contact is determined by the product of sliding velocity and the component of force that is tangential to the gear surface. The latter is linked to the normal force on the gear via the coefficient of friction. Within gear contacts the friction coefficient depends on a number of parameters, including pressure angle, speed, width, lubricant viscosity and roughness [**6**]. Therefore the coefficient of friction changes with rotational speed and contact load along the contact path. For an arbitrary meshing location on the contact tooth, the coefficient of friction can be given by

$$\mu_{\mathrm{c}} = 0.002 \left(\frac{F_{\mathrm{Nc}}}{b \times 0.001}\right)^{0.2} \times \left[\frac{2}{\cos\alpha (V_{1\mathrm{c}} + V_{2\mathrm{c}}) R_{\mathrm{Ec}} \times 0.001}\right]^{0.2} \eta^{-0.05} X_{\mathrm{R}} \tag{7}$$

Originally, equation (7) has been used to estimate a mean coefficient of friction and has been correlated from a number of experimental programmes [**7**]. However, following the comments in reference [**6**], in the present analysis it has been adopted to estimate the local friction coefficient within the contact. Its application will be discussed more fully later in the paper.

Within equation (7), for surfaces of identical roughness, the parameter X_{R} is given by

$$X_{\mathrm{R}} = 3.8 \left(\frac{S_{\mathrm{R}}}{d_1}\right)^{0.25}$$

For a surface roughness S_{R} of 0.6 μm Ra and pitch diameter of 79.95 mm, X_{R} assumes a value of 1.12. The dynamic viscosity of the lubricant, η, is expressed as [**8**]

$$\eta = 10^{-6} \rho \left(\exp\left\{ \exp\left[21.54 - \frac{3.54 \log(\theta_{\mathrm{B}} + 273)}{\log(2.718286)} \right] \right\} - 0.6 \right) \tag{8}$$

In equation (8), the bulk temperature (θ_{B}) is calculated assuming the application of lubricant via a spray system [**7**].

2.1.3 *Frictional heat flux along the contact path*

The heat fluxes on the contact area of the pinion and gear generated by frictional sliding of the meshing teeth can be expressed respectively as

$$q_{1\mathrm{c}} = \beta q_{\mathrm{c}} = \beta \gamma \mu_{\mathrm{c}} p_{\mathrm{Nc}} V_{\mathrm{gc}} \times 10^6$$
$$q_{2\mathrm{c}} = (1 - \beta) q_{\mathrm{c}} = (1 - \beta) \gamma \mu_{\mathrm{c}} p_{\mathrm{Nc}} V_{\mathrm{gc}} \times 10^6 \tag{9}$$

The heat conversion factor γ is defined to be 0.95 and the partition constant of the heat flux between the contact areas of the two engaged teeth, β, is 0.5. These

values have been used in the present study in the absence of better information. However, as more precise data becomes available it may be incorporated readily into the model. Every tooth on the pinion or gear receives the heat input once over one revolution during rotations. Thus the averaged frictional heat flux for the meshing areas on the pinion and gear teeth over one revolution can be expressed as

$$q_{1\text{ave}} = \frac{2a/(V_{1\text{c}} \times 1000)}{60/n_1} q_{1\text{c}},$$
$$q_{2\text{ave}} = \frac{2a/(V_{2\text{c}} \times 1000)}{60/n_2} q_{2\text{c}} \tag{10}$$

2.2 Heat transfer coefficients

2.2.1 Heat transfer coefficient on gear surfaces

Heat is removed from the gear through convection from the sides and from the surfaces of the teeth flanks. Heat loss from the gear side can be approximated by convective losses from rotating discs and a fling-off model may be used for the tooth flank (see section 2.2.3). The convective heat transfer coefficients on the gear sides were calculated by using the results derived from a rotating circular disc [**9**]. The heat transfer coefficient of the gear surface changes with radial location depending on the flow type. The type of flow around the surface is divided into laminar, transitional and turbulent flow respectively, corresponding to the range of rotational Reynolds number values. The heat transfer coefficients for the different flow regimes are presented in terms of Nusselt and Reynolds numbers based on the local radius.

For rotating discs, laminar flow corresponds to a Reynolds number Re of less than 2×10^5 and the heat transfer coefficient, h_s, can be expressed as [**4**, **10**]

$$h_\text{s} = \frac{k_\text{f}\, Nu}{r_\text{c}} = 0.308 k_\text{f} (m+2)^{0.5} Pr^{0.5} \left(\frac{\omega}{\nu_\text{f}}\right)^{0.5} \tag{11}$$

The transitional flow corresponds to a Reynolds number between 2×10^5 and 2.5×10^5; an estimation of heat transfer coefficient in this regime refers to the investigation based on the measurements conducted by Popiel and Boguslawski [**11**]:

$$h_\text{s} = \frac{k_\text{f}\, Nu}{r_\text{c}} = 10 \times 10^{-20} k_\text{f} \left(\frac{\omega}{\nu_\text{f}}\right)^4 r_\text{c}^7 \tag{12}$$

When the Reynolds number is greater than 2.5×10^5, the flow around the gear surface becomes turbulent. The heat transfer coefficient can be determined using an integral energy equation derived by Dorfman [**12**]:

$$h_\text{s} = \frac{k_\text{f}\, Nu}{r_\text{c}}$$
$$= 0.0197 k_\text{f} (m+2.6)^{0.2} Pr^{0.6} \left(\frac{\omega}{\nu_\text{f}}\right)^{0.8} r_\text{c}^{0.6} \tag{13}$$

2.2.2 Surface heat transfer coefficient in an air and oil mist environment

The heat transfer coefficients derived above are based on a single-phase flow which may not be valid under conditions when the method of cooling for the gear is jet lubrication. Two-phase flow applies to the gear surface and the surrounding flow on the surfaces consists of a mixture of air and oil. A simple method was introduced to evaluate the influence of the air and oil mist on the heat transfer coefficient at the gear surfaces [**13**].

The notion of a synthesized single-phase flow was used to account for the effects of the mixture of air and oil, the location of the gear surface and operational conditions on the heat transfer coefficient. The properties of the synthesized fluid are defined as

$$\zeta_\text{f} = [\alpha_\text{a} + (1-d)\alpha_\text{o}]\zeta_\text{a} + \alpha_\text{o} d \zeta_\text{o} \tag{14}$$

where ζ_f, ζ_a, ζ_o are the properties of the synthesized single-phase fluid, the air and the cooling oil respectively. This includes properties such as kinematic viscosity, thermal conductivity, Prandtl number, etc. The variable d is included as a weighting factor to be determined experimentally for evaluating the effects of operational conditions on the flow. The parameters α_a and α_o are defined as average volume fractions occupied by the air and oil on the gear surface respectively. If the flow on the gear surface is largely controlled by air flow, $\alpha_\text{a} = 1$, $\alpha_\text{o} = 0$; conversely, $\alpha_\text{a} = 0, \alpha_\text{o} = 1$ applies to the flow determined principally by oil. The following linear relation is applied:

$$\alpha_\text{a} + \alpha_\text{o} = 1$$
$$\alpha_\text{a} = 1 - \frac{2r_\text{c}}{d_\text{a}}$$
$$\alpha_\text{o} = \frac{2r_\text{c}}{d_\text{a}} \tag{15}$$

In the central area of the gear surface, $r_\text{c} \approx 0$, the flow is determined mainly by the air, the influence of oil on the flow is neglected; if the radius r_c reaches the tip of the gear surface, the flow is determined by a mixture of air and oil. Using the synthesized properties defined in equations (14), the heat transfer coefficient in the air and oil mist environment at the gear surfaces can be estimated.

2.2.3 *Heat transfer coefficient on the tooth flank*

The method of cooling for the gear transmission in this research is jet cooling, by which the oil is supplied to each tooth flank once per revolution. This process was characterized as intermittent fling-off cooling with a sequence of transient and forced heat convection as described by DeWinter and Blok [**14**]. An approach for estimating the heat transfer coefficient on the tooth flank has been developed based on a model where the frictional heat is withdrawn from the tooth flank by a centrifugal fling-off process. By establishing the general energy equation for transient and forced convective heat transfer in a flowing incompressible liquid together with the definition of dimensionless variables, the normalized cooling capacity, q_{tot}, has been obtained [**14**, **15**]. The heat transfer coefficient, h_{tc}, can be expressed as

$$h_{\text{tc}} = \frac{\sqrt{\omega}}{2\pi}\sqrt{k\rho c}\left(\frac{v_0 H_{\text{c}}}{\alpha r_{\text{c}}}\right)^{1/4} q_{\text{tot}} \tag{16}$$

The fling-off mechanism is appropriate for a short period following the mesh contact and ideally this may be replaced subsequently by forced convection as the gear teeth rotate within the gearbox enclosure. On reviewing the literature, the flow over ribbed surfaces gave the closest approximation. However, these were not considered to be appropriate since the rib and teeth geometry were sufficiently different and therefore, for the purpose of this study, this component of heat loss was neglected.

2.3 Finite element simulation

2.3.1 *Heat equation and boundary conditions*

As a result of the frictional sliding heating between the teeth engaged in a pair of gears, the temperature of the tooth surfaces changes during the meshing process. However, the bulk temperature of the gears can achieve a thermal equilibrium after many cycles at a fixed load. After reaching an equilibrium state, the temperature changes in the gear tooth body during one revolution are very small. This is because most of the heat generated on the surfaces is taken away by the cooling lubricant and the time is very limited for heat conduction from the surface into the body under high-speed operations. By assuming every single tooth of the gear follows the same cycle, i.e. heating, then convective cooling and conduction, the heat balance of the gear can be analysed by establishing a single-tooth model (Fig. 3). Applying the law of conservation of energy and Fourier's law, the energy equation of the single-tooth

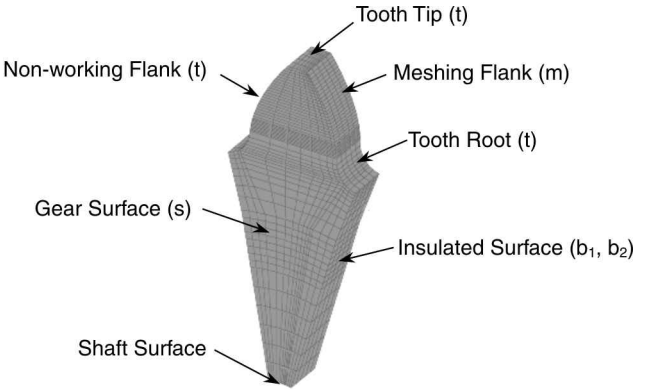

Fig. 3 FE mesh of single-tooth model with the definition of gear surfaces

model can be expressed as

$$k\left(\frac{\partial^2 T}{\partial x^2} + \frac{\partial^2 T}{\partial y^2} + \frac{\partial^2 T}{\partial z^2}\right) = \rho c \frac{\partial T}{\partial t} \tag{17}$$

where temperature, $T = T(x, y, z, t)$, changes with time t and position x, y, z. Based on Newton's law of cooling and Fourier's law, convective boundary conditions for the different surfaces are specified as follows:

$$\begin{aligned} -\left.\frac{\partial T}{\partial n}\right|_{\text{m}} &= h_{\text{m}}(T - T_{\text{oil}}) + q_{\text{F}} \\ -\left.\frac{\partial T}{\partial n}\right|_{\text{t}} &= h_{\text{t}}(T - T_{\text{oil}}) \\ -\left.\frac{\partial T}{\partial n}\right|_{\text{s}} &= h_{\text{s}}(T - T_{\text{a}}) \end{aligned} \tag{18}$$

The insulated heat condition on the symmetrical surfaces of the gear model is written as

$$\left.\frac{\partial T}{\partial n}\right|_{\text{b1}} = \left.\frac{\partial T}{\partial n}\right|_{\text{b2}} = 0 \tag{19}$$

2.3.2 *Steady state finite element temperature analysis*

By dividing the temperature $T(x, y, z, t)$ into the bulk temperature $T_{\text{B}}(x, y, z)$ and the flash temperature $T_{\text{F}}(x, y, z, t)$ and considering the flash temperature to change with time cyclically, the temperature changes expressed by equation (17) over a cycle time t_{T}, i.e. from t to $t + t_{\text{T}}$, are represented as

$$\begin{aligned} &\int_t^{t+t_{\text{T}}} k\left(\frac{\partial^2 T_{\text{B}}}{\partial x^2} + \frac{\partial^2 T_{\text{B}}}{\partial y^2} + \frac{\partial^2 T_{\text{B}}}{\partial z^2}\right) \text{d}t + \int_t^{t+t_{\text{T}}} k \\ &\quad \times \left(\frac{\partial^2 T_{\text{F}}}{\partial x^2} + \frac{\partial^2 T_{\text{F}}}{\partial y^2} + \frac{\partial^2 T_{\text{F}}}{\partial z^2}\right) \text{d}t \\ &\quad = \rho c \int_t^{t+t_{\text{T}}} \left(\frac{\partial T_{\text{B}}}{\partial t} + \frac{\partial T_{\text{F}}}{\partial t}\right) \text{d}t \end{aligned} \tag{20}$$

Considering $\partial T_B/\partial t = 0$, $T_B > 0$, $T_F > 0$ and $T(t) = T(t + t_T)$, then

$$\int_t^{t+t_T} \frac{\partial T}{\partial t}\,dt = \int_t^{t+t_T} \frac{\partial T_F}{\partial t}\,dt = 0 \tag{21}$$

Substituting equations (20) and (21) into equation (17) gives the steady state equation for the bulk temperature of the single-tooth model. This steady state approximation is appropriate when the conditions are such that there is negligible local heat removal when the tooth is not in engagement. This is appropriate under the condition of high rotational speed since the time interval for local heat removal is short:

$$k\left(\frac{\partial^2 T_B}{\partial x^2} + \frac{\partial^2 T_B}{\partial y^2} + \frac{\partial^2 T_B}{\partial z^2}\right) t_T = 0,$$

$$\text{i.e. } \frac{\partial^2 T_B}{\partial x^2} + \frac{\partial^2 T_B}{\partial y^2} + \frac{\partial^2 T_B}{\partial z^2} = 0 \tag{22}$$

Clearly, by following a traditional approach, a knowledge of the bulk temperature coupled with a flash temperature model will allow the instantaneous flank temperature to be calculated.

2.4 Modelling procedure

Based on the above formulations, a computer program was developed to implement analysis and calculation for a given gear configuration and operational conditions. The relevant parameters obtained from the program were then input into the FE model as boundary conditions for temperature analyses. A flow chart of the modelling procedure is presented in Fig. 4.

2.5 Models and definitions

The geometrical data of a spur gear transmission are listed in Table 1 and are the same as the design in a test rig, so the modelling results can be compared with experimental measurements. The gears are also designed with tip relief. Finite element meshes of the pinion and gear for tooth temperature analysis were established by creating tokens based on parametric definitions of gear profiles and preliminary data [**16**]. As shown in Fig. 3, the FE mesh for the pinion is presented, consisting of 3100 three-dimensional eight-node linear rectangular elements with a total of 4176 nodes. The material of the pinion and gear in the FE simulation was 665M17 (EN-34) steel. The mechanical and thermal properties are given in Table 2. This gear geometry was chosen since experimental data had been gathered for this gear set. Practically, gears of lower module are used in high-speed applications and a separate experimental study on such gears has been carried out. This gear set was case-hardened and ground to a surface finish of 0.6 μm Ra. The influence of this finish is included in the equation defining X_R. The lubrication oil used is Mobil Jet II and its properties are listed in Table 3.

To establish the quality of the simulation, results are compared with measurements conducted as part of an experimental programme. To summarize the salient points from the programme, the surface temperature of the pinion tooth was inferred from infrared camera

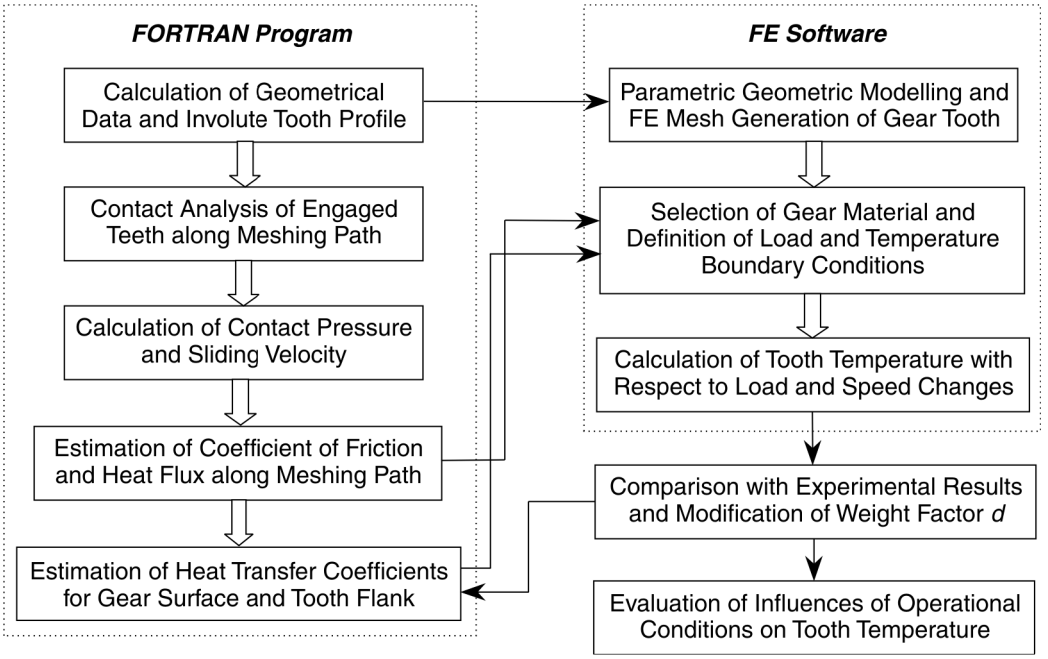

Fig. 4 Modelling procedure of tooth temperature analysis

Table 1 Gear geometric data

Number of teeth	$Z_1 = 15$, $Z_2 = 16$	Module	$m = 5.33\,\text{mm}$
Pressure angle	$\alpha = 26^\circ$	Tooth width	$b = 4.775\,\text{mm}$
Pitch diameter	$d_1 = Z_1 m = 79.95\,\text{mm}$	Tip diameter	$d_{a1} = 90.61\,\text{mm}$
	$d_2 = Z_2 m = 85.28\,\text{mm}$		$d_{a2} = 95.94\,\text{mm}$
Root diameter	$d_{f1} = 66.63\,\text{mm}$	Base circle diameter	$d_{b1} = d_1 \cos\alpha = 71.86\,\text{mm}$
	$d_{f2} = 71.96\,\text{mm}$		$d_{b2} = d_2 \cos\alpha = 76.65\,\text{mm}$
Centre distance	$A = 82.55\,\text{mm}$	Shaft diameter	$d_{s1} = 12.7\,\text{mm}$
Pitch	$p = 16.74\,\text{mm}$	Base pitch	$p_b = p \cos\alpha = 15.05\,\text{mm}$
Transverse contact ratio	$\varepsilon_\alpha = 1.3382$	Transverse path of contact	$g_\alpha = \varepsilon_\alpha p_b = 20.14\,\text{mm}$

Table 2 Material properties of pinion 665M17 (EN-34) steel

Young's modulus	Poisson's ratio	Expansion coefficient	Density	Thermal conductivity	Specific heat
185.42 GPa	0.3	$1.1 \times 10^{-5}\,\text{K}^{-1}$	$7870\,\text{kg/m}^3$	41.8 W/m K	493 J/kg K

Table 3 Properties of lubricating oil (Mobil Jet II)

Viscosity v (m^2/s)	Conductivity k (W/m K)	Specific heat c (J/kg K)	Density ρ (kg/m^3)
30×10^{-6} (40 °C)	0.1337 (37.8 °C)	2000 (90°)	998
5.5×10^{-6} (100 °C)	0.1278 (93.3 °C)		
	0.1157 (200 °C)		

Table 4 Definitions of load cases in the FE simulation

	Case A	Case B	Case C	Case D	Case E	Case F	Case G
Torque of driving shaft (N m)	17.4	26	35	43	52	61	73
Maximum of normal pressure (N/mm)	106.6	159.3	214.5	263.5	318.7	373.8	447.4

measurements and tooth temperature was measured using thermocouples. The thermocouples were embedded into the gears and held in place using glue, as the aim of the experiments was to measure a steady state temperature. The signals were routed to a data acquisition system via a slip ring unit. The infrared camera was positioned and directed to measure temperature on the flank surface of the gear 180° downstream from the contact point. To do so it was necessary to calibrate the camera to account for the oil spray within the chamber and the background temperature within the chamber itself. This was achieved by using the oil supply temperature as a black body reference and establishing a relationship with the tooth temperature for a range of oil temperatures (see Fig. 5) [**17**]. During the course of the experiments, oil was delivered on to the driving flank in the downward direction of meshing at a flowrate of 380 ml/min through a small nozzle under conditions that allowed a spray to form in the chamber. The gear sump was drained immediately to prevent the accumulation of lubricant and the penalty of churning losses.

FE models with different combinations of operating conditions were established for evaluating the influences of load, speed, heat transfer coefficient, ambient and oil inlet temperatures, and gear geometry on tooth temperature variations. Rotational speeds were assumed to be 2000–10 000 r/min and the tooth normal load was varied in the range 106.6–447.4 N/mm, thereby covering the operational conditions for the experimental measurements of tooth temperature. The loads applied in the FE simulations were defined by load cases A to G; values of the torque and the maximum normal pressure for these cases are listed in Table 4. Based on the experimental data, the oil inlet and ambient temperatures were assumed to be 90 and 70 °C respectively.

3 RESULTS AND DISCUSSION

3.1 Frictional heat flux

By applying the computer program that has been developed as part of this research, the sliding velocity,

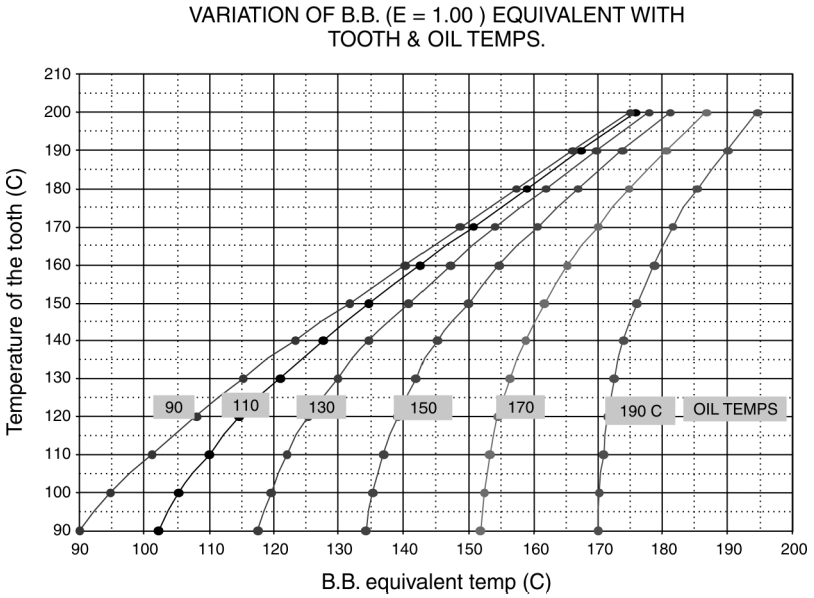

Fig. 5 Calibration characteristics for the infrared camera [**17**]

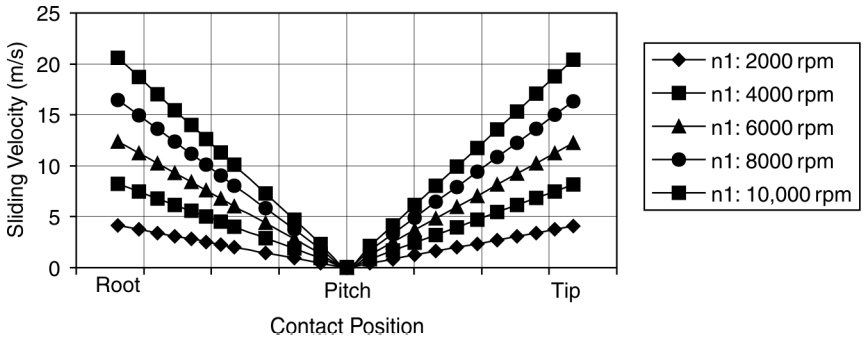

Fig. 6 Distributions of sliding velocity along the contact path

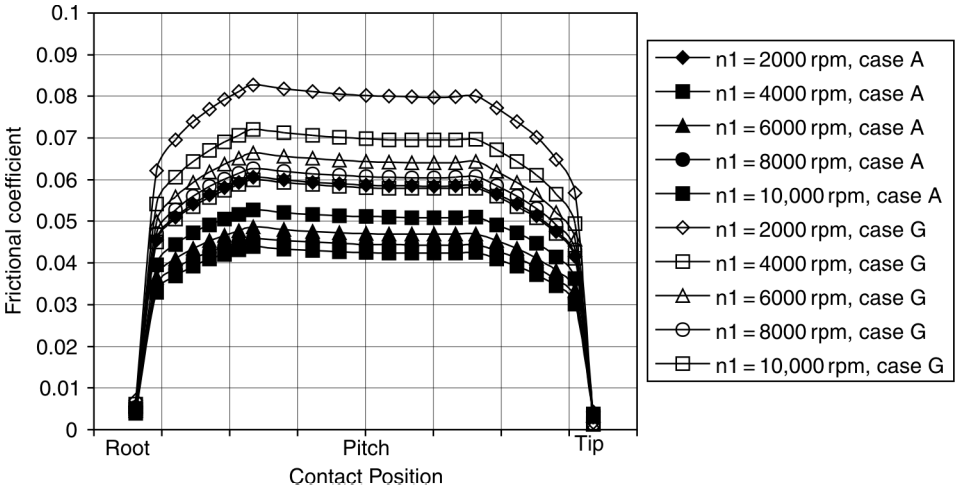

Fig. 7 Coefficients of friction along the contact path for load cases A and G

coefficient of friction and contact pressure in the meshing teeth along the contact path were calculated, as shown in Figs 6, 7 and 8. The velocity is shown in modulus form in Fig. 6, since it is used for computing power loss. Also in this instance, the sliding velocity at the tip and root are symmetrical about the pitch line since the velocity ratio is close to unity. The variation of the sliding velocity changes with the rotational speed

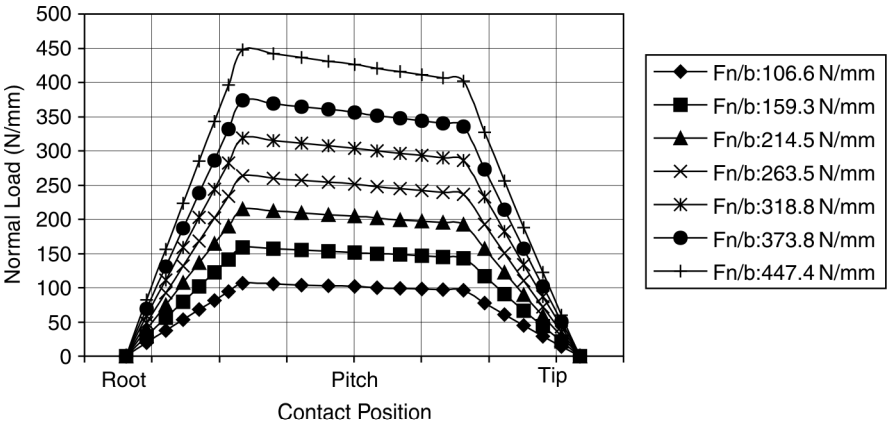

Fig. 8 Normal load distributions along the contact path for load cases A to G

and position of the teeth contact, while by using equation (7), the coefficient of friction is mainly dependent on the applied load, as well as on the rotational speed and the position through the contact (see Figs 6 and 7). Also, as shown in Fig. 8, the tooth contact remains fixed since tooth deflection is neglected. The current work focuses on thermal behaviour only and a full thermomechanical analysis could be an extension of this study.

The trends in Fig. 7 capture the increase in coefficient with the increase in load and the coefficient falls as the meshing speed increases. However, at the tip and root points, the model suggests that the friction coefficient falls to a value that is close to zero. This may be compared with results published by Crook [**18**], where even at the lightest load the friction coefficient retains a finite level. This points to a discrepancy and a limitation in the application of equation (7) to estimate the local friction coefficient. To explore the impact on dissipation, the friction coefficient at the initial tip and root contact was set to the value at the adjacent nodes, thereby achieving a finite level. The impact on dissipation in the contact was insignificant in this case due to the relief in the tooth tip profile. This avoids sudden changes in normal contact pressure (Fig. 8). In the case where tip relief is not used, the dissipation at the start of the contact is also likely to be high. However, the remaining calculations retain the application of equation (7).

The combined effects of load, speed and friction produced a non-uniform heat flux over the tooth working flanks, as shown in Fig. 9. It is clear that the changes in heat flux distribution on the tooth flank becomes significant for the range of applied loads, especially at higher speeds with heavy loading conditions (Fig. 10). It produces the maximum heat flux at the tooth dedendum, i.e. shortly after the tooth of the pinion enters the contact; another peak value of heat flux occurs on the tooth addendum. This resulted from the combined effects of sliding velocity and contact pressure distribution over the tooth flank. The heat flux is zero at the pitch line because of the pure rolling action in the meshing teeth at this instant.

3.2 Heat transfer coefficients

Heat transfer coefficients for the pinion and gear under different rotational speeds were calculated using the developed computer program. The results showed that the values of heat transfer coefficients changed over a large range for the speed envelope explored. This reflects on the operational conditions of lubrication and the nature of the local flow. The heat transfer coefficients for the surface and pinion tooth flank are shown in Fig. 11. The heat transfer coefficients on the surfaces [derived using equation (11) or (12) or (13)] increase rapidly with radius and rotational speed dependent on flow type and mixture of air and oil on the surface. In contrast, the average heat transfer coefficients on the tooth flank [derived using equation (16)] increase gently with the radius of tooth height under different speed conditions.

3.3 Tooth temperature

As the heat transfer coefficient for the surfaces is affected by the operational conditions of lubrication, a weight factor, d, is defined to reflect practical conditions in experiments. An initial value of factor d was assumed and FE analysis was implemented. By comparing FE temperature results with experimental measurements, the value of d was adjusted to minimize the deviation between the two. After several iterations of this process, the factor d (used for calculating the surface heat transfer coefficient) was defined to be 0.3–0.7 for rotational speeds between 2000 and 10 000 r/min.

Example temperature distributions over the whole surface of the pinion tooth are illustrated in Fig. 12, where the rotational speeds are 2000, 6000 and 10 000 r/min with a range of applied normal loads from 106.6 to 447.4 N/mm respectively. The surface temperature was

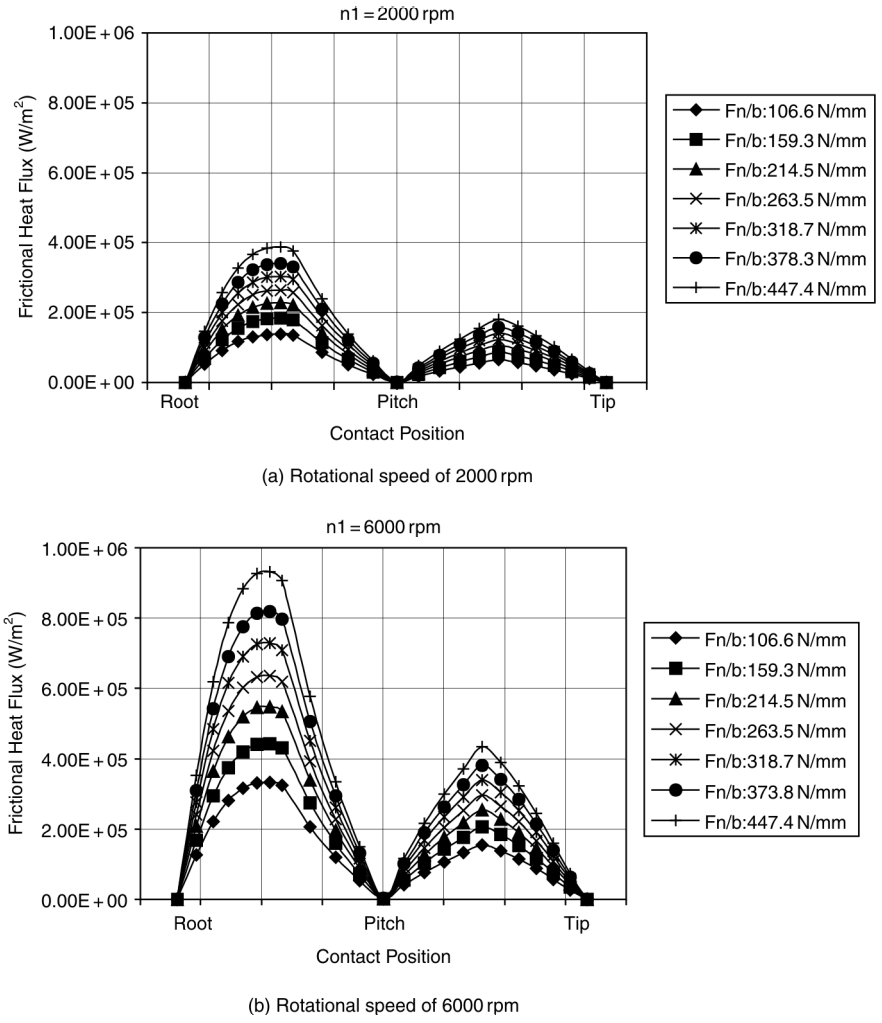

Fig. 9 Frictional flux distributions of the pinion along the contact path

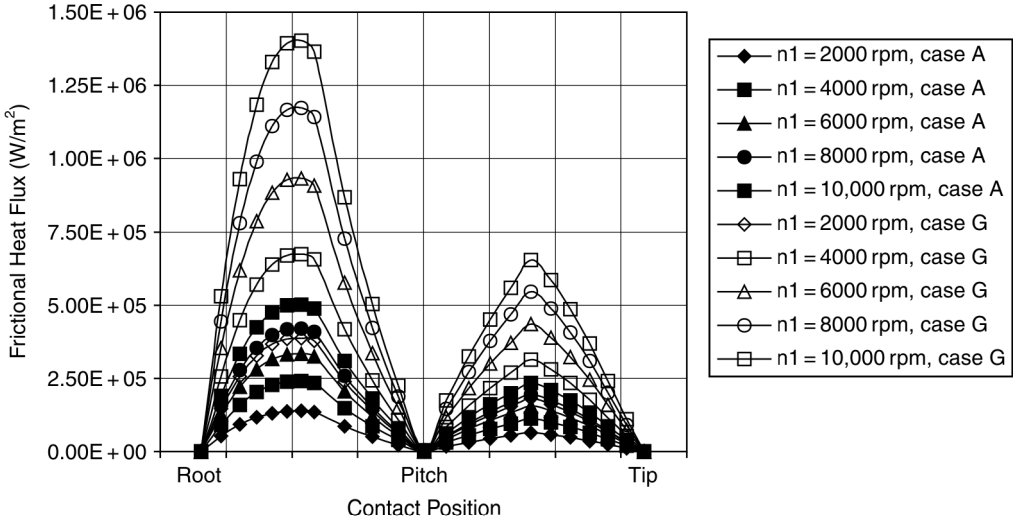

Fig. 10 Effects of load and speed on the frictional heat flux of the pinion

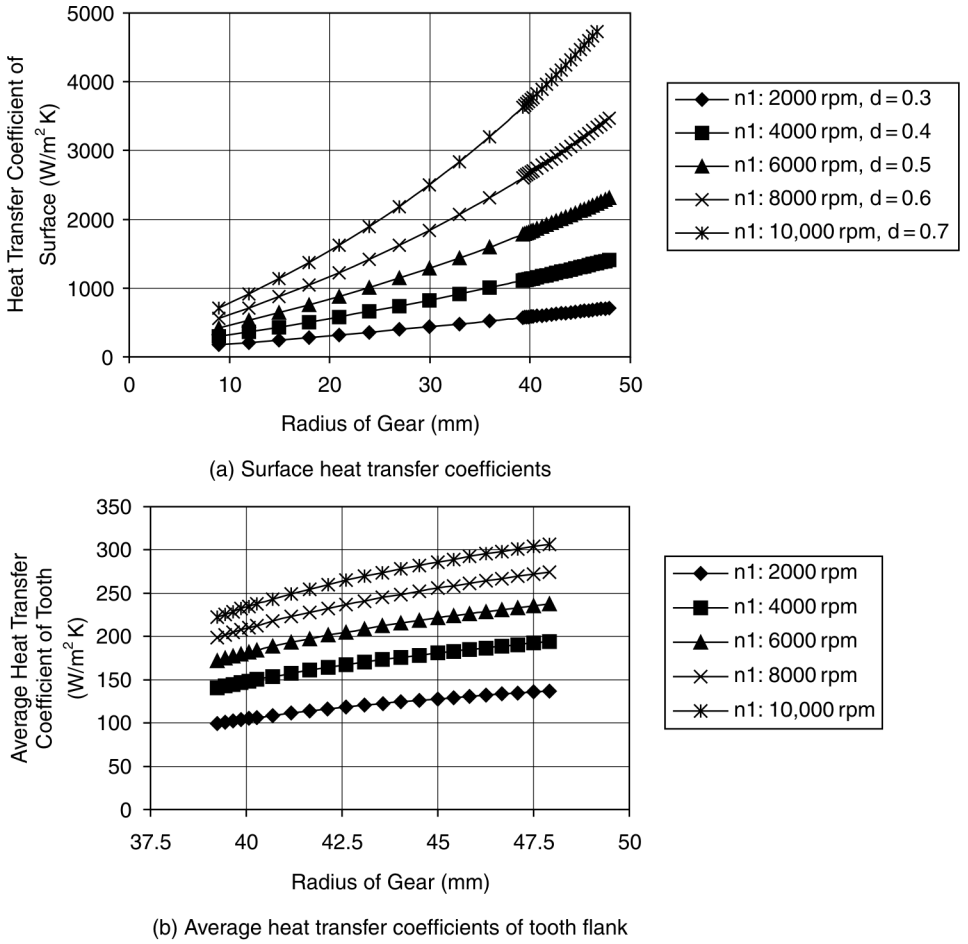

Fig. 11 Heat transfer coefficients of the pinion

substantially higher than the body temperature, especially when a combination of high load and speed was applied. The frictional heat generated at the flank was conducted into the tooth body and transferred from the tooth surfaces. However, the frictional heat flux distribution still resulted in the maximum temperature occurring at the dedendum close to the pitch line; this is expected since the shearing energy is dissipated over a smaller distance. Temperature differences in the pinion tooth became obvious when greater loads were applied at higher speeds, as shown in Figs 12b and c.

For comparison with experiments, the FE results were derived at locations on the surface (point A), in the tooth (point B) and in the body (point C) (Fig. 13). Values of surface and tooth temperatures are in good agreement with measurement results for most of the range of loads applied. The discrepancy in surface temperature between the FE analysis and the experiment is less than 7 per cent when normal loads are lower than 320 N/mm for rotational speeds of 2000, 4000 and 6000 r/min. The deviations in tooth temperature are smaller than 5 per cent for the operational conditions evaluated. However, the body temperatures derived by the FE analysis have obvious differences from the measurements, especially for higher speeds, which is most probably caused by the neglect of bearing heating in the vicinity of the driving shaft.

As shown in Fig. 13, the temperature increases with the rotational speed, but the difference in surface temperature between the FE results and measurements increases as the load increases. This may occur for a number of reasons. The first is because the maximum surface temperature becomes much larger than the average temperature of the tooth flank when the applied load is higher, while the temperature recorded in experiments may be more representative of the average flank temperature. A second reason may be attributed to the contact friction model. At high loads, the friction coefficient may be overestimated in the simulations and this will also lead to a higher temperature being predicted. This, together with a more complete exploration of heat removal by the two phase flows, is an area that requires further research attention.

Distributions of surface temperature on the tooth flank for the pinion over a range of rotational speeds and loads are shown in Fig. 14. Due to the non-uniform distribution of frictional heat flux, two peak values of surface temperature occur on the tooth flank. This trend

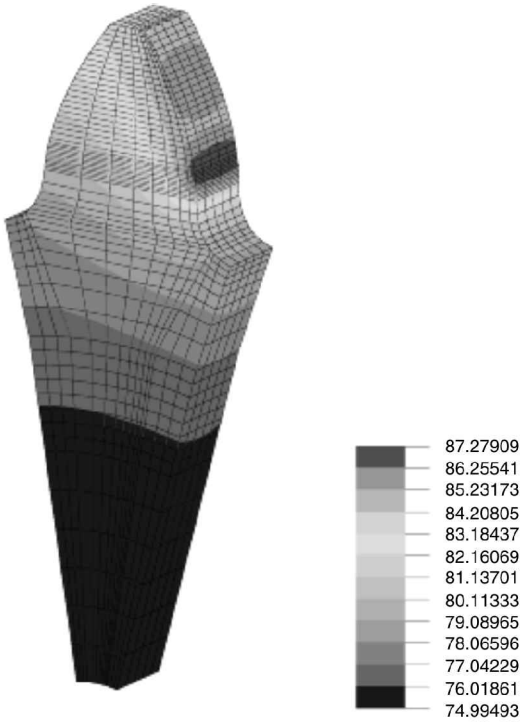

(a) Normal load of 106.6 N/mm at rational speed of 2000 rpm

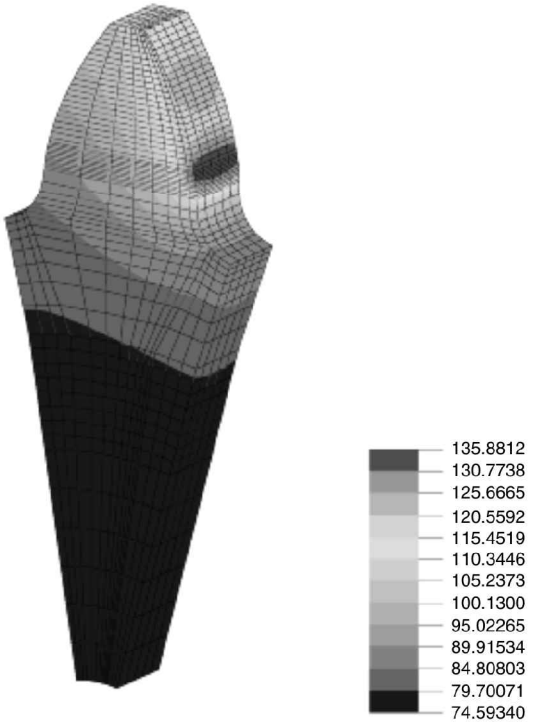

(b) Normal load of 447.4 N/mm at rational speed of 6000 rpm

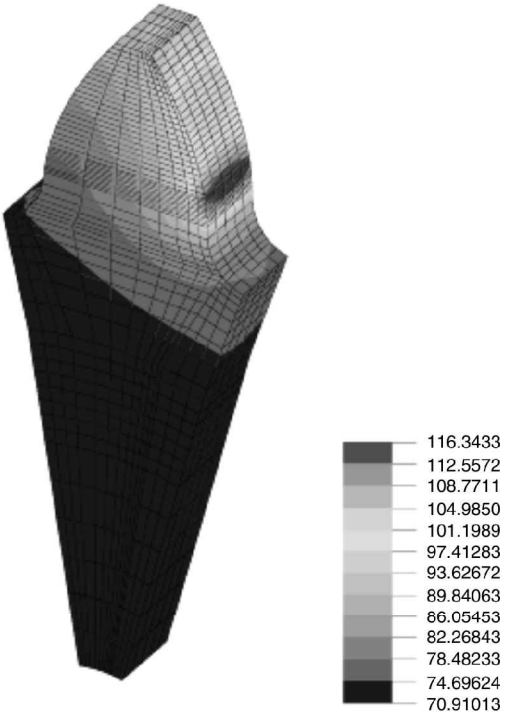

(c) Normal load of 214.5 N/mm at rational speed of 10,000 rpm

Fig. 12 Temperature distributions of the pinion tooth

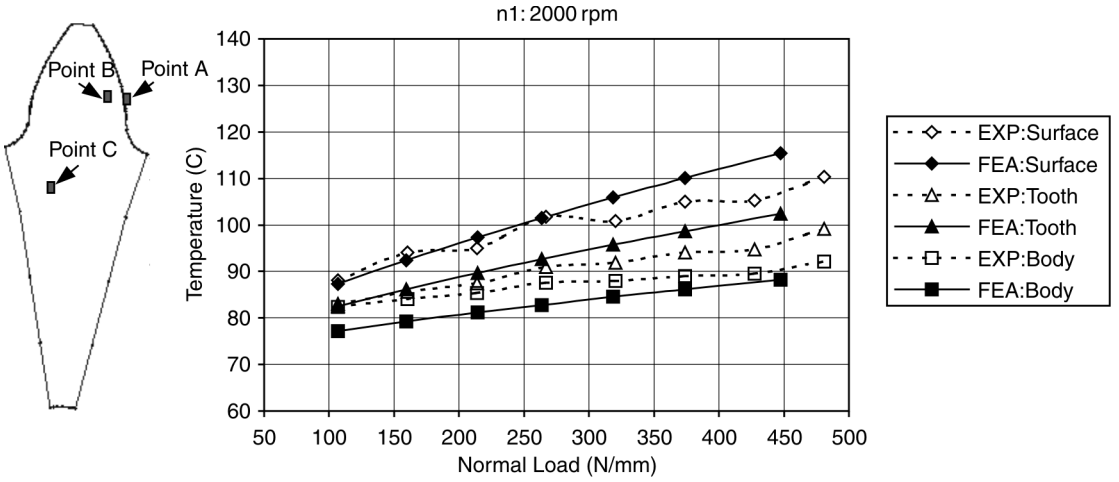

(a) Rotational speed of 2000 rpm

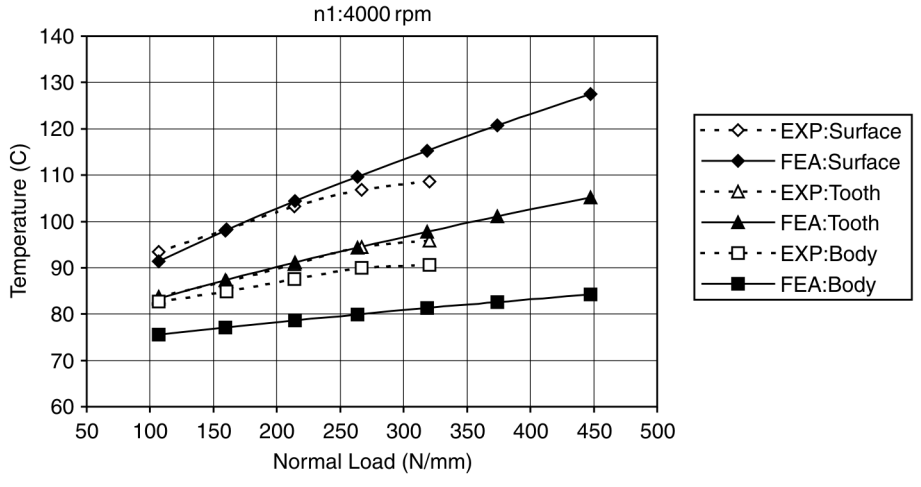

(b) Rotational speed of 4000 rpm

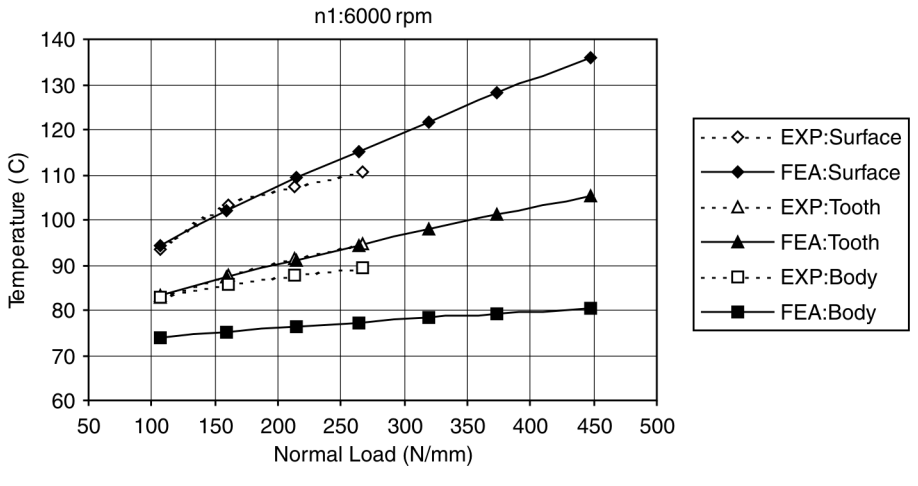

(c) Rotational speed of 6000 rpm

Fig. 13 Temperature variations with load and comparison with experiments

becomes more self-evident at higher speeds and greater loads. As can be seen from Fig. 15, the maximum surface temperatures for load cases A and G increase by 12.9 and 28.4 per cent respectively as the rotational speed changes from 2000 to 10 000 r/min. However, the load has a more significant effect on the maximum surface temperature in comparison with the rotational speed. The maximum surface temperatures for rota-

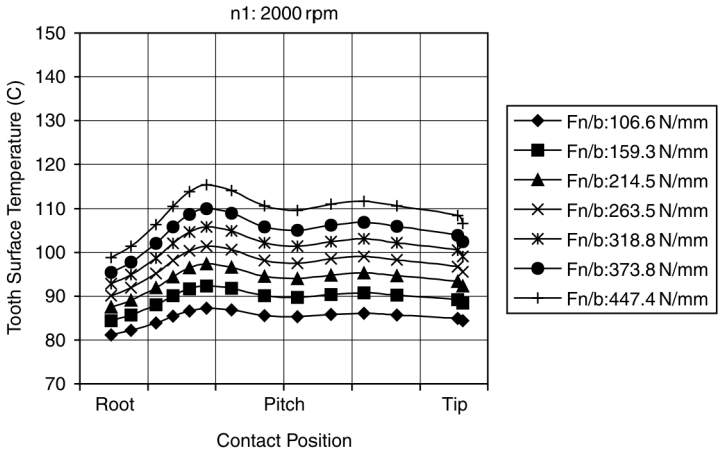

(a) Rotational speed of 2000 rpm

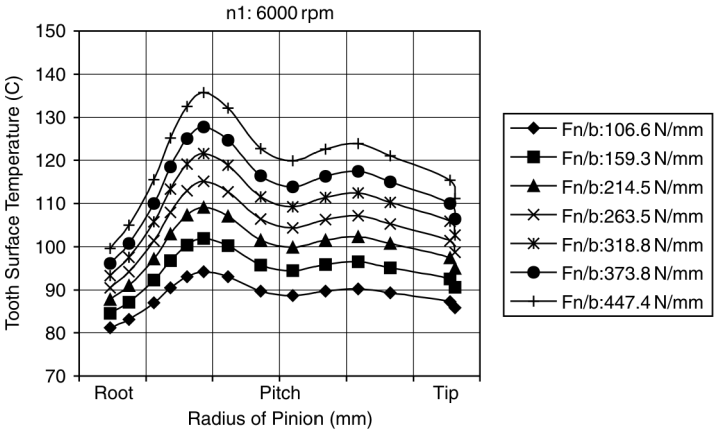

(b) Rotational speed of 6000 rpm

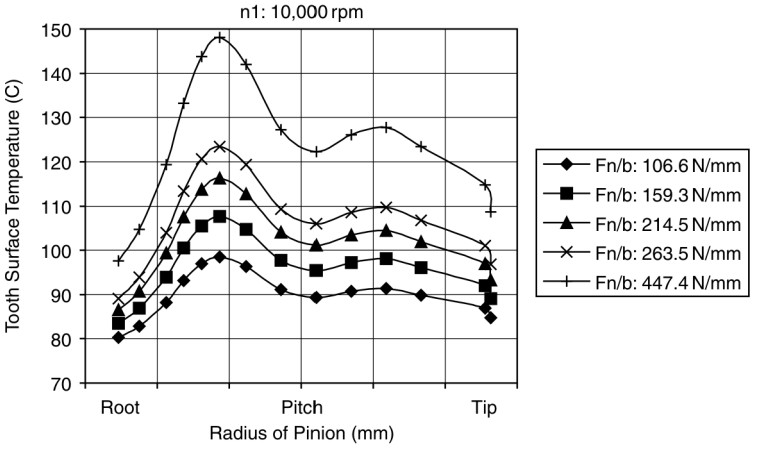

(c) Rotational speed of 10,000 rpm

Fig. 14 Distributions of surface temperature on the tooth flank

tional speeds of 2000, 4000, 6000, 8000 and 10 000 r/min increase by 32.2, 39.4, 44, 47.5 and 50.4 per cent respectively as the normal load increases from 106.6 to 447.4 N/mm. This is a reflection of the friction coefficient model that has been used, which displays a higher sensitivity with respect to load [**7**, **18**].

Correlations may be derived to enable a more rapid calculation of maximum surface temperatures. Follow-

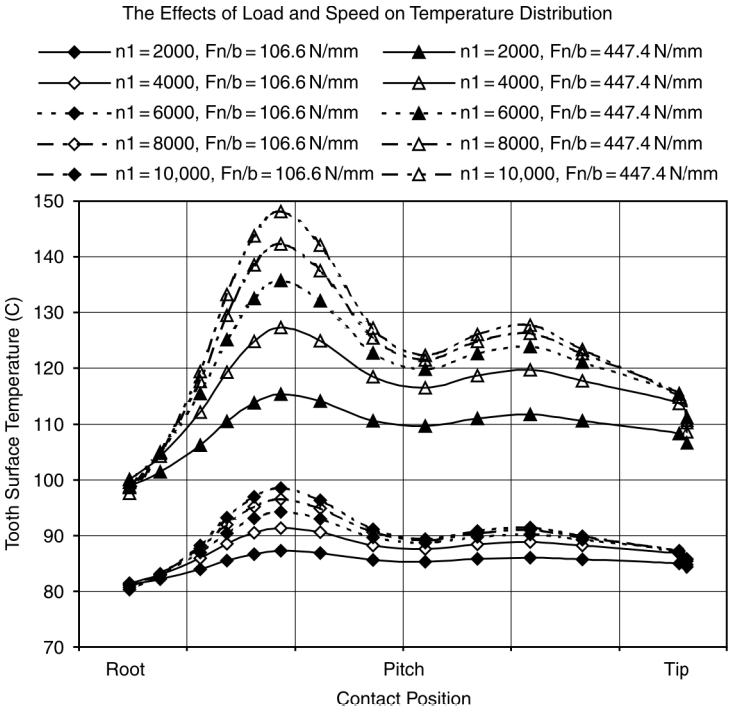

Fig. 15 Effects of load and speed on surface temperature distributions

Table 5 Constants in exponential equations for the surface temperature of the pinion

Load (N/mm)	106.6	159.3	214.5	263.5	447.4
C_L	35.14	31.02	28.75	27.27	26.1
M	0.19	0.22	0.25	0.27	0.28
Speed (r/min)	2000	4000	6000	8000	10 000
C_S	49.16	44.94	41.99	40.04	35.42
N	0.075	0.095	0.111	0.122	0.155

ing investigation and based on the FE simulations, variations in the maximum surface temperature of the pinion with load and speed can be expressed by the relationships

$$T_{s,\,max}\begin{cases} = C_S(n_1)^n \\ = C_L\left(\frac{F_n}{b}\right)^m \end{cases} \tag{23}$$

Values of constants of C_S, n and C_L, m were calculated based on the FE analyses and are presented in Table 5. Thus the maximum surface temperature under arbitrary loads and speeds can be estimated using these simple expressions for the gear configuration used.

3.4 Sensitivity of surface temperature

Changes in tooth configuration, heat transfer coefficients and oil inlet and ambient temperatures will affect the tooth temperature. To evaluate temperature sensitivity to relevant factors, FE simulations were performed to investigate variations of surface and tooth temperatures with changes in tooth width, module, surface and tooth flank heat transfer coefficients, heat flux and ambient and oil inlet temperatures.

3.4.1 Tooth width

Figure 16 shows that the maximum surface temperatures of the pinion increase linearly with load for speeds of 2000 and 6000 r/min when the tooth width is defined to be 0.9, 2 and 3 times the module respectively. The original width of the pinion tooth in the gear design is 0.9 times the module. As seen in Fig. 16, the increase of tooth width causes large rises in the maximum surface temperature, especially at higher speeds and loads. At a rotational speed of 6000 r/min with a normal load of 373.8 N/mm, the maximum temperatures increase by 19.7 and 35.5 per cent respectively when the width is 2 and 3 times the module. The increases are smaller at 2000 r/min and are 15.9 and 29.1 per cent respectively. This is because heat generated on the flank is not dissipated so easily to the cooling oil when the tooth width increases. This arises due to the increased length of the conduction path to the gear side. It also confirms the significant influence of heat removal from the gearwheel side.

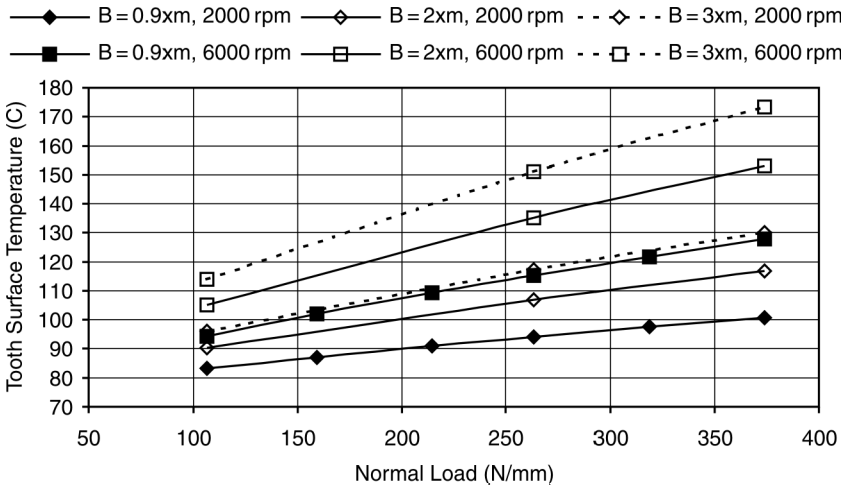

Fig. 16 Effect of tooth width on the maximum surface temperature

3.4.2 *Tooth module*

Changes in the tooth module also cause temperature variations due to changes of tooth size, as shown in Fig. 17, where the module is defined to be 5.3, 8 and 10 mm respectively. As shown in Fig. 17a, the surface temperature of the tooth increases with the module, especially at the higher speed when the same values of heat flux and heat transfer coefficients derived for the original module tooth (5.3 mm) were applied. This is due to the increase in tooth size (and volume), which results in changes in heat conduction. However, when the analyses were run for the 8 and 10 mm modules while maintaining the load calculations for the 5.3 mm module, the combined effects of the changes of module cause a smaller rise, or even a decrease, in surface temperature. As can be seen from Fig. 17b, the surface temperature increases by 2.5 per cent for a normal load of 447.4 N/mm at 6000 r/min when the module increases from 5.3 to 8 mm, but it decreases by 5.1 per cent when the module is 10 mm. This is because the changes of module cause a rise in the heat transfer coefficient as well as an increase in load capacity. While keeping the same values of normal load on the tooth, the surface temperature is dependent on the thermal balance of heating and heat transfer on the tooth. It is obvious that the changes in module result in a larger impact on surface temperature at the higher speed.

3.4.3 *Ambient and oil inlet temperatures*

The changes in ambient temperature result in an increase or decrease of surface temperature, as shown in Fig. 18. The percentage in surface temperature variations is about ± 6.5 per cent while the ambient temperature changes by ± 10 per cent of the original definition for the range of loads and speeds applied. It becomes clear that the ambient temperature has a proportional impact on the tooth temperature under the steady state FE simulation. Hence, the correct ambient temperature specification is a key requirement for predicting tooth temperature accurately.

Changes in oil inlet temperature produced less than ± 1 per cent variation of surface temperature when the oil temperature was increased or decreased by ± 10 per cent. This is because the FE simulation is based on a steady state analysis; the heat transfer coefficient on the tooth flank was averaged over one revolution and was relatively smaller in comparison with the surface coefficient. Thus the influence of oil temperature is not significant.

3.4.4 *Frictional heat flux*

The variations of the maximum surface temperature resulting from the frictional heat flux are dependent on the rotational speed and load sustained. The maximum change of temperature is about ± 4.5 per cent when the changes in heat flux are defined to be changed by ± 10 per cent of the calculated values, as shown in Fig. 19. This confirms the importance of precision in the calculation of the heat flux for defining the heat load conditions in the FE simulations.

3.4.5 *Heat transfer coefficients*

Figure 20 shows the variations of the maximum surface temperature with the changes of ± 10 per cent in the surface heat transfer coefficient. The percentage of temperature variation ranges from ± 0.77 to ± 2.95 per cent as a function of speed and load. The expected reason for the small temperature variation is that the estimated heat transfer coefficient is already at a high level; thus a ± 10 per cent change in the surface heat transfer coefficient does not produce significant variations of temperature. The high value also links the

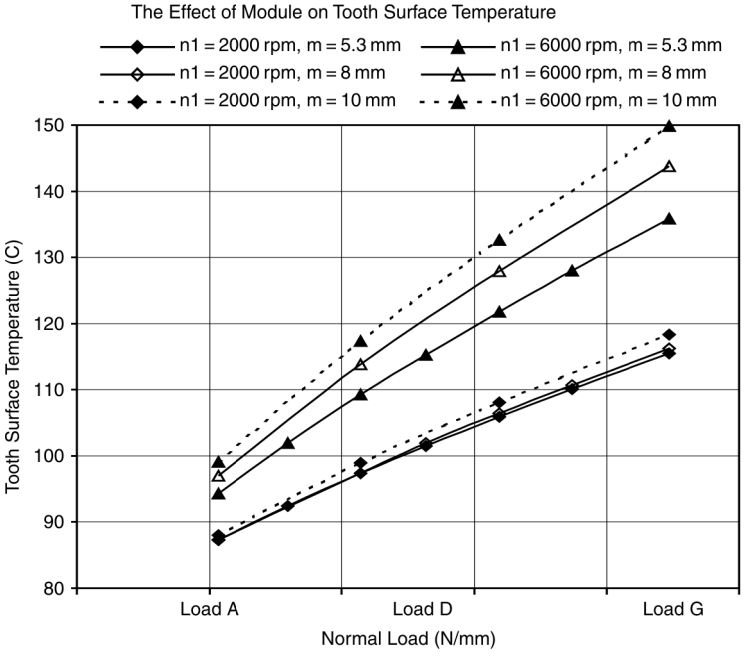

(a) Effect due to the change of tooth size

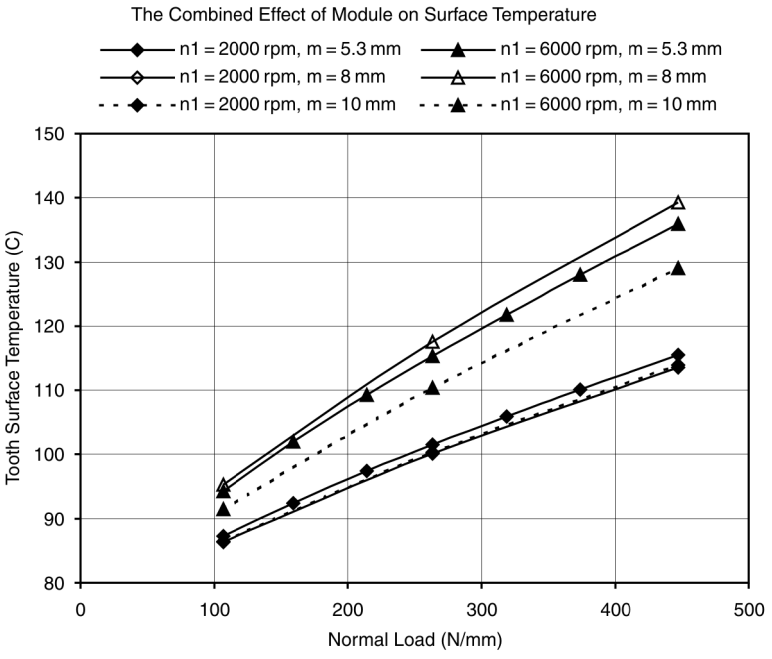

(b) Combined effects due to the changes of tooth size, heat transfer coefficients and load

Fig. 17 Effects of tooth module on the maximum surface temperature

surface temperature to the ambient temperature value, which has been shown to have a proportional effect in Fig. 18. Also the average heat transfer coefficient on the flank is at a lower value in comparison with the surface heat transfer coefficient. As a consequence, ± 10 per cent changes of flank heat transfer coefficient caused minimal variations of surface temperature of less than ± 1 per cent.

4 CONCLUSIONS

From the modelling procedure developed and analytical results discussed in the previous sections, the following conclusions have been drawn:

1. An analysis and modelling procedure for predicting thermal behaviour and determining the tooth tem-

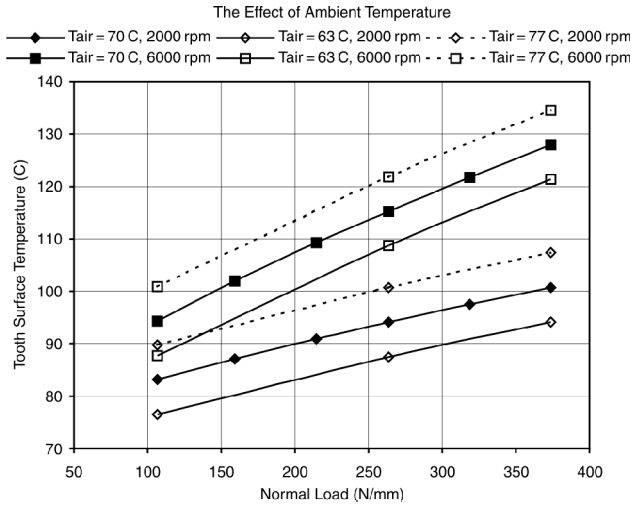

Fig. 18 Effect of ambient temperature on the maximum surface temperature

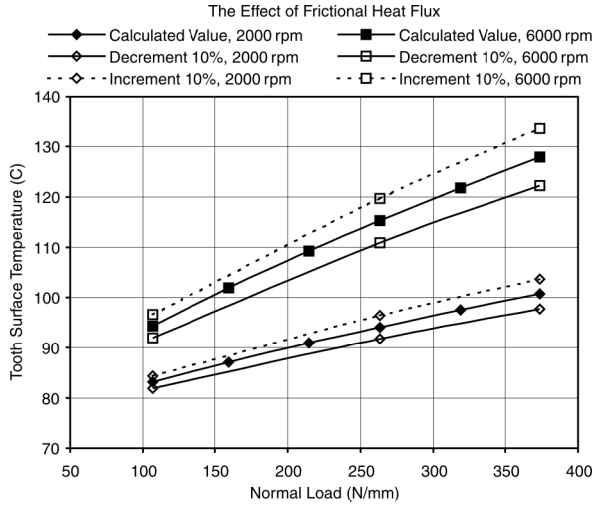

Fig. 19 Effect of frictional heat flux on the maximum surface temperature

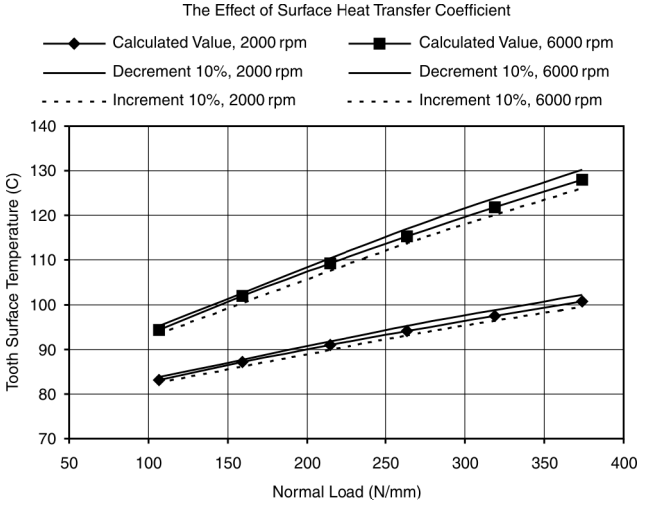

Fig. 20 Effect of surface heat transfer coefficient on the maximum surface temperature

perature has been established by theoretical calculations and finite element analyses.

2. The frictional heat flux along the contact path of the meshing teeth and heat transfer coefficients on the gear surface and tooth flank were estimated. Steady state tooth temperatures were predicted, provided that basic experimental results were known to define boundary conditions for the FE model.
3. FE results of tooth surface temperatures are in good agreement with the experimental measurements and the general deviations are less than 7 per cent. The tooth temperature is mainly determined by load and speed as well as gear geometrical configuration. Load has a more significant effect on the tooth temperature in comparison with the rotational speed, reflecting the dominance of load in determining the coefficient of friction in the contact.
4. A sensitivity analysis of the surface temperature revealed that tooth geometry has an important impact on tooth temperature variations and distributions, especially the changes of tooth width. Ambient temperature under operational conditions is an essential parameter to define boundary conditions in FE models. The 10 per cent change of the surface heat transfer coefficient has a small impact on the balanced surface temperature, while the changes of the heat transfer coefficient of the tooth flank and oil temperature do not produce obvious influences on the surface temperature. Precise calculation of the frictional heat flux is required to predict tooth temperature accurately.

ACKNOWLEDGEMENTS

The authors acknowledge the financial support of the European Union under the INTRANS Project and the support of Turbomeca and Eurocopter, France.

REFERENCES

1 **Townsend, D. P.** and **Akin, L. S.** Analytical and experimental spur gear tooth temperature as affected by operating variables. *Trans. ASME, J. Mech. Des.*, January 1981, **103**, 219–226.
2 **Wang, K. L.** and **Cheng, H. S.** A numerical solution to the dynamic load, film thickness and surface temperatures in spur gears, Part I: analysis. *Trans. ASME, J. Mech. Des.*, January 1981, **103**, 177–187.
3 **Wang, K. L.** and **Cheng, H. S.** A numerical solution to the dynamic load, film thickness and surface temperatures in spur gears, Part II: results. *Trans. ASME, J. Mech. Des.*, January 1981, **103**, 188–194.
4 **Patir, N.** and **Cheng, H. S.** Prediction of the bulk temperature in spur gears based on finite element temperature analysis. In ASLE/ASME Lubrication Con-

ference, Kansas, Missouri, October 1977, Preprint 77-LC-38–2.

5 **Terauchi, Y.** and **Mori, H.** Comparison of theories and experimental results for surface temperature of spur gear teeth. *Trans. ASME, J. Engng for Industry*, February 1974, 41–50.

6 **Castro, J.** and **Seabra, J.** Scuffing and lubricant film breakdown in FZG gears, Part I: analytical and experimental approach. *Wear*, 1998, **215**, 104–113.

7 **Winter, H.** and **Michaelis, K.** Scoring load capacity of gears lubricated with EP-oils. In AGMA technical paper, Fall Technical Meeting, Montreal, October 1983, AGMA technical paper.

8 **Garcia, A. H.** Thermal effects in high speed gear transmissions. MSc degree thesis, University of Wales Swansea, September 1999.

9 **Gardon, G., Astarita, T.** and **Carlomagno, G. M.** Infrared heat transfer measurements on a rotating disk. *Opt. Diagnostics in Engng*, 1996, **1**(2), 1–7.

10 **Hartnett, J. P.** and **Deland, E. C.** The influence of prandtl number on the heat transfer from rotating non-isothermal disks and cones. *Trans. ASME, J. Heat Transfer*, 1961, **C83**, 95–96.

11 **Popiel, C. Z. O.** and **Boguslawski, L.** Load heat-transfer coefficient on the rotating disk in still air. *Int. J. Heat Mass Transfer*, 1975, **18**, 167–170.

12 **Dorfman, L. A.** *Hydrodynamic Resistance and the Heat Loss of Rotating Solids*, translated 1963 (Oliver and Boyd).

13 **Patir, N.** Estimate of the bulk temperature in spur gears based on finite element temperature analysis. MSc degree thesis, Northwestern University, Evanston, Illinois, May 1976.

14 **DeWinter, A.** and **Blok, H.** Fling-off cooling of gear teeth. *Trans. ASME, J. Engng for Industry*, February 1974, **96**(1), 60–70.

15 **van Heijningen, G. J. J.** and **Blok, H.** Continuous as against intermittent fling-off cooling of gear teeth. *Trans. ASME, J. Lubric. Technol.*, October 1974, 529–538.

16 *ELFEN User Manual, Version 2.7*, 1998 (Rockfield Software Limited).

17 Web page: www.landinst.com/infr.

18 **Crook, A. W.** The lubrication of rollers. IV. Measurements of friction and effective viscosity. *Phil. Trans. R. Soc.*, 1962, **255A**, 281–312.

